Supporting information

Impact of Interface Disorder on the Crystallization and Charge Transport of Conjugated Polymer Thin Films in Organic Field-Effect Transistors

Abhirup Das[1], Krishnendu Maity[2], Samik Mallik[3], Riya Sadhukhan[1], Rajdeep Banerjee[1], Suman Kalyan Samanta[2], Dipak K. Goswami[1]

[1]*Organic Electronics Laboratory, Department of Physics, Indian Institute of Technology Kharagpur, Kharagpur – 721302, India*

[2]*Department of Chemistry, Indian Institute of Technology Kharagpur, Kharagpur – 721302, India*

[3]*School of Nano Science and Technology, Indian Institute of Technology Kharagpur, Kharagpur – 721302, India*

***Email: dipak@phy.iitkgp.ac.in**

Synthesis of Isoindigo-BTBT:

M1 (1.35 g) and **M2** (700 mg) were taken in a Schlenk flask under a nitrogen atmosphere with 10 mL of anhydrous toluene. Tris(dibenzylideneacetone)dipalladium(0) ($Pd_2(dba)_3$) (56.6 mg) and tri(o-tolyl) phosphine ($P(o\text{-}tol)_3$) (37.6 mg) were added as a toluene solution so that the total volume of toluene becomes 30 mL. The tube was purged with nitrogen for 30 min by bubbling nitrogen. The reaction was stirred at 90 °C for 3 days under a nitrogen atmosphere. Then, tributyl(phenyl)stannane (0.5 mL) was added, and the mixture was stirred overnight (12.0 h), followed by the addition of 2 mL bromobenzene and further stirred for 8.0 h. The resulting mixture was poured into methanol and stirred for 1.0 h. The precipitates were filtered and dissolved in chloroform and precipitated in acetone and stirred for 2 h. The dark precipitates were filtered off and subjected to Soxhlet extraction for 3 days successively with methanol, acetone, and hexane (1 day for each solvent) for the removal of remaining monomers, oligomers, and catalytic impurities. After that, the polymer was extracted with chloroform and precipitated in methanol. The precipitate was dried under vacuum at 50 °C to obtain the desired polymer in 80% yield (1.16 g). ^{1}H NMR (400 MHz, $CDCl_3$) δ 9.12 (br, 2H), 7.46 (br, 7H), 6.2 (br, 6H), 3.76 (br, 4H), 1.99 (br, 4H), 1.228 (br, 169H), 0.89 (br, 12H). M_n, 14,800; M_w/M_n = 1.5. UV ($CHCl_3$), λ_{max} (ε_{max}): 358 nm, 476 nm.

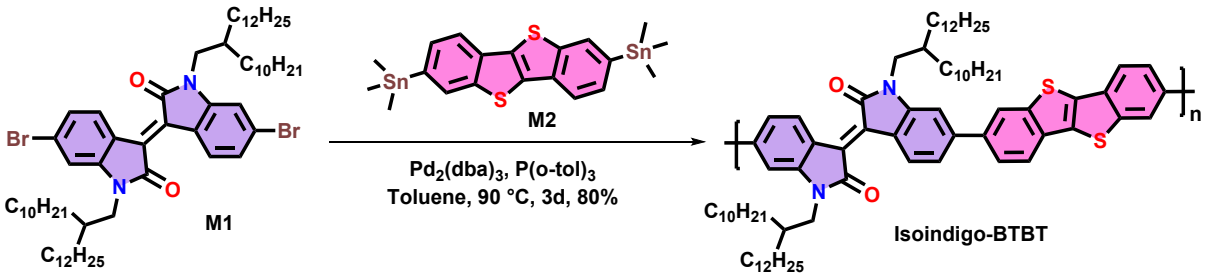

Scheme 1. Synthetic route for Isoindigo-BTBT through Pd-catalyzed Stille polymerization.

NMR spectrum of Isoindigo-BTBT:

The broadening of ^{1}H-NMR signals (as shown in FIG S1) observed in these polymers provided clear evidence of successful polymerization. This broadening is attributed to the restricted motion of protons along the polymer chains, indicative of the extended conjugation and the rigidity of the backbone. Furthermore, the broad signals also confirmed the formation of strong π-stacking interactions between the aromatic rings of the conjugated backbones.

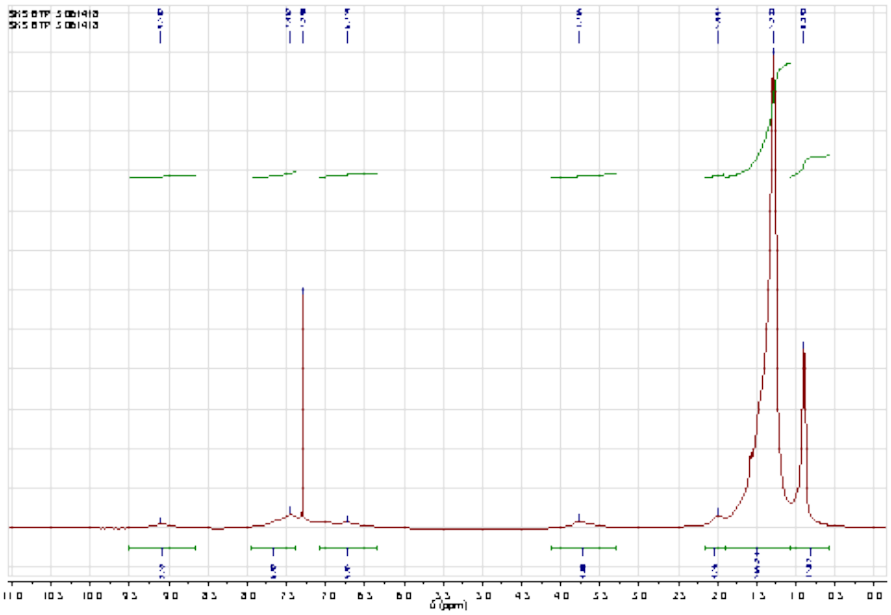

FIG. S1: ^{1}H-NMR spectrum of Isoindigo-BTBT in $CDCl_3$.

Gel Permeation Chromatography (GPC) data of Isoindigo-BTBT:

GPC was utilized (as shown in FIG S2) to assess the weight average molecular weight (M_w) and polydispersity index (PDI) of the synthesized polymers, employing polystyrene as an internal standard and chlorobenzene as the eluent at 35 °C. M_w and PDI values are 27,173 g.mol^{-1} and 2.7, respectively, which suggests the successful formation of the polymer.

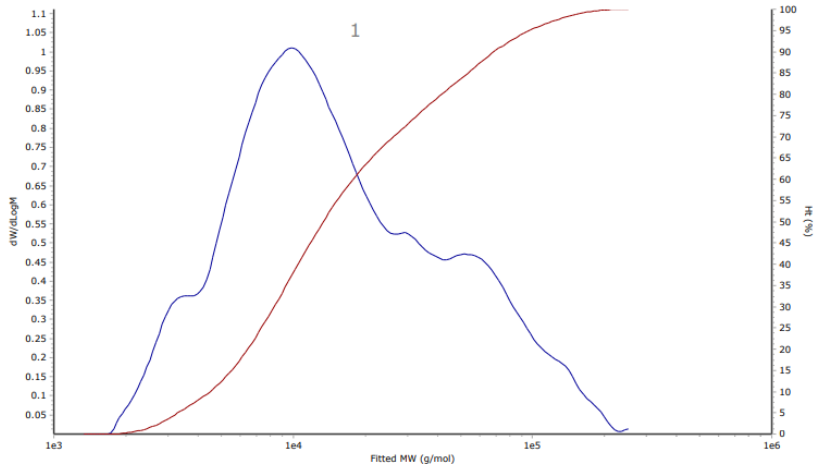

FIG. S2: GPC data of Isoindigo-BTBT in $CDCl_3$.

Cyclic Voltammetry (CV) analysis of Isoindigo-BTBT:

The cyclic voltammetry (CV) analysis curve of the Isoindigo-BTBT polymer is shown in Fig. S3, providing insight into its electronic properties. From the CV data, the lowest unoccupied molecular orbital (LUMO) energy level of the synthesized polymer was determined to be -3.36 eV. This value was calculated based on the onset of the reduction peak in the CV curve, which reflects the material's electron affinity.

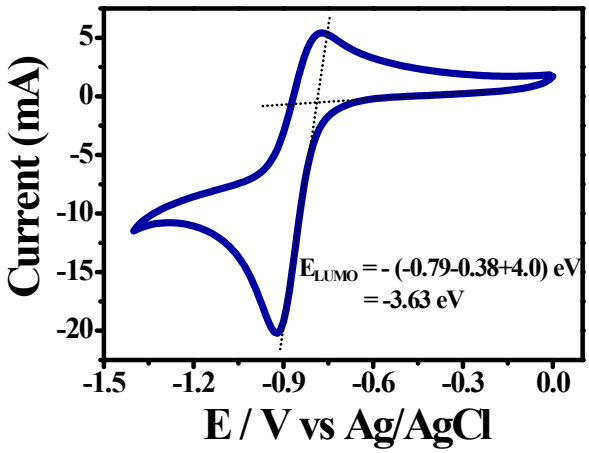

FIG. S3: CV analysis of Isoindigo-BTBT.

Energy minimized structure of Isoindigo-BTBT:

The energy-minimized structure of Isoindigo-BTBT is shown in Fig. S4. The HOMO distribution across the conjugated backbone of the donor-acceptor polymer demonstrates effective delocalization, confirming its p-type semiconducting behaviour. This characteristic makes it a promising candidate for applications in organic field-effect transistors and other electronic devices.

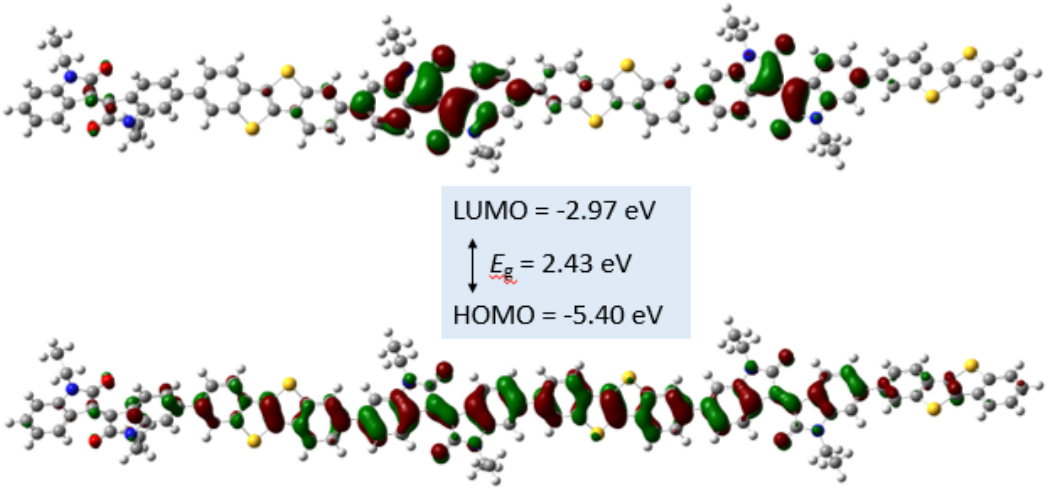

FIG. S4: Energy minimized structure of Isoindigo-BTBT. A high-lying LUMO energy level (-3.63 eV), and the HOMO distribution along the conjugated backbone of the donor-acceptor polymer emphasize its p-type semiconducting nature.

UV-vis absorption spectroscopy of Isoindigo-BTBT:

The UV-Vis absorption spectra of the material, shown in Fig. S5(a), exhibit a maximum absorbance at 473 nm within the visible region, along with a broader absorption extending up to 720 nm. The corresponding Tauc plot, depicted in Fig. S5(b), was used to estimate the material's optical bandgap. By extrapolating the linear portion of the Tauc plot to the x-axis, the bandgap was determined to be 1.77 eV. This optical behaviour highlights the material's potential for applications in optoelectronic devices requiring visible-light absorption.

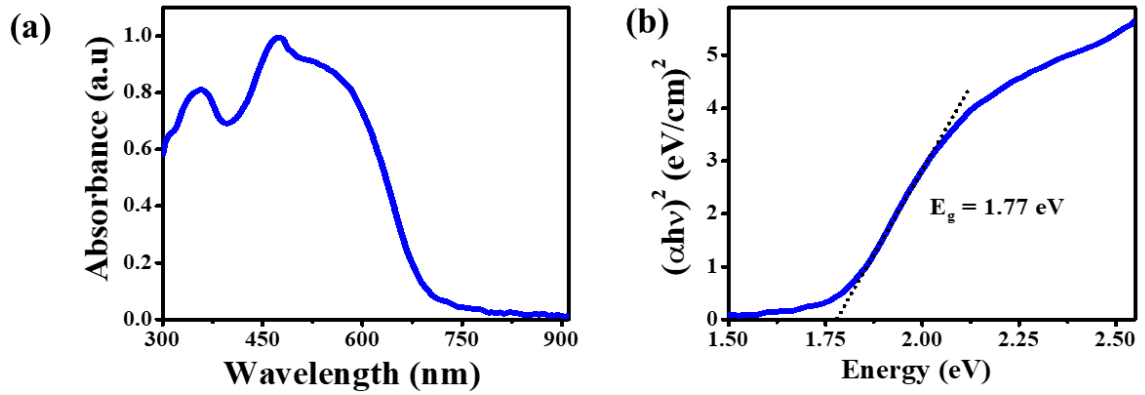

FIG. S5: (a) UV-Vis absorption spectra of Isoindigo-BTBT, and (b) The band gap (E_g) calculation from the Tauc plot. The bandgap was determined to be 1.77 eV by extrapolating the linear portion of the Tauc plot to the x-axis.

Variation of d-spacing, thickness, and roughness of the film with annealing temperature:

XRR analysis reveals a consistent shift in the Bragg peak position with increasing annealing temperature up to 125 °C. This corresponds to a decrease in d-spacing from 2.33 (±0.01) nm to 2.15 (±0.02) nm, as shown in Fig. S6(a). Additionally, annealing at 125 °C leads to a slight reduction in film thickness from 24.05 (±0.05) nm to 23.79 (±0.06) nm, as illustrated in Fig. S6(b). Concurrently, the surface roughness exhibits a linear decline from 2.07 (±0.05) nm to 1.39 (±0.04) nm, as seen in Fig. S6(c). These observations indicate structural densification and surface smoothing of the film upon thermal treatment, suggesting enhanced molecular packing with annealing temperature.

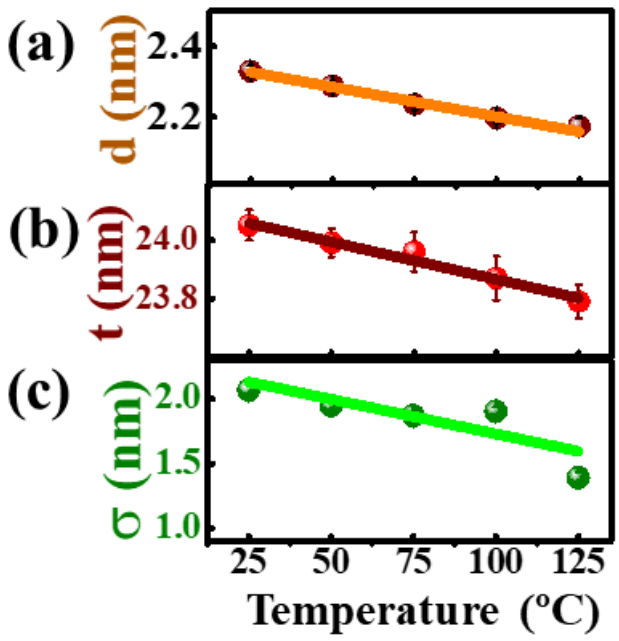

FIG. S6: Variation of (a) d-spacing, (b) thickness (t), (c) roughness (σ) of the Isoindigo-BTBT film at various annealing temperatures extracted by fitting of the XRR data.

Determining the optimal structural model and parameter values from XRR fitting

To demonstrate the uniqueness of the electron density profile at 125 ºC, we have considered all plausible internal structural configurations of the film—namely, fully ordered, surface-disordered, substrate interface-disordered, and both interfaces-disordered. The corresponding theoretical XRR curves for each case are presented in Figure S7(a) and S7(b). Among these, only the model featuring disorder at both interfaces yields a theoretical fit that closely matches the experimental data, whereas the other configurations fail to do so.

In addition, we systematically varied the parameters—film thickness, surface and interface roughness, and electron density (ρ_e)—as shown in Figure S7(c–k), and calculated the corresponding χ^2 values for each case. The parameter set that produced the lowest χ^2 value was selected as the optimal fit.

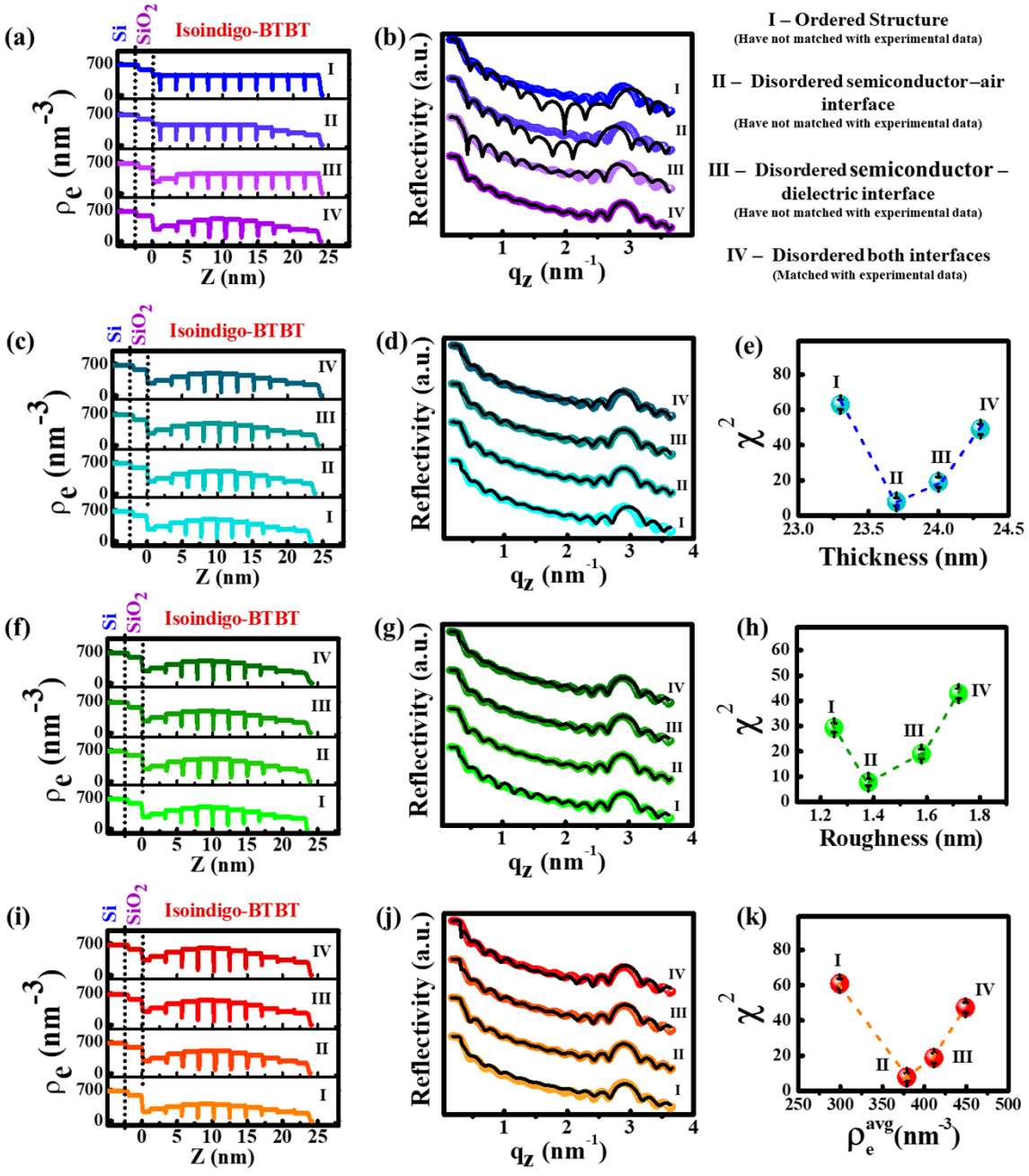

FIG. S7: (a) and (b) Electron density profiles (EDPs) of the annealed sample, showing the corresponding fitted XRR data for different structural configurations: ordered film, surface disordered, substrate interface disordered, and both interfaces disordered. (c)–(e) EDPs of the sample for varying thickness, with their corresponding fitted data and χ^2 values. (f)–(h) EDPs of the sample for varying surface roughness, accompanied by their corresponding fitted data and χ^2 values. (i)–(l) EDPs of the sample for varying electron density, with the corresponding fitted data and χ^2 values.

Differential Scanning Calorimetry (DSC)- Thermo-Gravimetric Analysis (TGA) of Isoindigo-BTBT:

The DSC-TGA measurement data, shown in Fig. S7, reveal the thermal transitions of the material. The violet curve represents the DSC heat flow for the polymer sample, highlighting key thermal events. The first dip at 87 °C corresponds to the glass transition temperature (T_g), indicating the onset of polymer softening. A distinct peak at 182 °C marks the crystallization temperature (T_c), signifying the formation of ordered polymer domains. The minima at 322 °C represent the melting temperature (T_m), where crystalline regions transition to the amorphous phase. Finally, a sharp drop at 380 °C, associated with significant weight loss in the TGA green curve, denotes the degradation temperature (T_d), indicating the thermal decomposition of the polymer. These results provide comprehensive insights into the material's thermal stability and phase transitions.

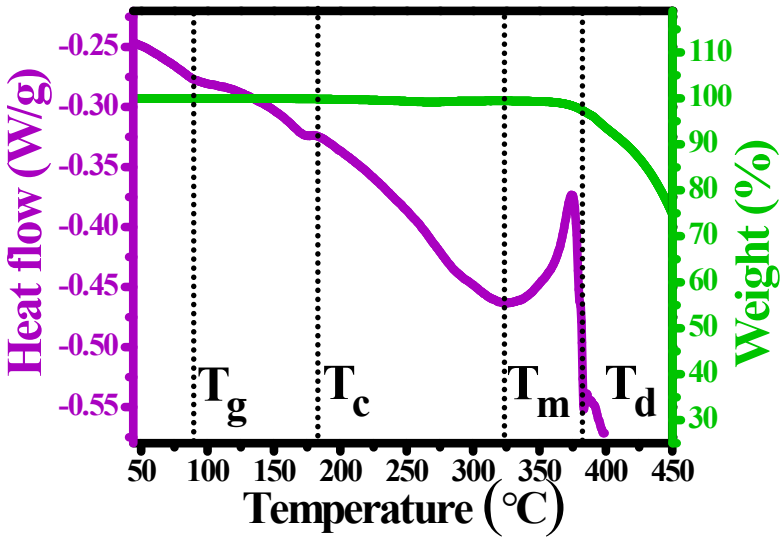

FIG. S8: Thermal analysis of the Isoindigo-BTBT polymer in the form of bulk. The violet curve represents the heat flow obtained from the DSC measurement of the polymer sample. The DSC curve shows thermal transitions, including T_g at 87 °C, T_c at 182 °C, and T_m at 322 °C. A sharp drop at 380 °C indicates degradation (T_d), confirmed by the corresponding weight loss depicted in the TGA curve, as indicated by the green line.

Thickness measurement of the film with 5 mg/ml polymer concentration:

Due to the high roughness of the 5 mg/mL film, Kiessig fringes were not visible in the XRR curve [Fig. S8(a)], making it unsuitable for thickness estimation. In Fig. S8(b), the AFM image shows the spin-coated film on the left side, while the Si-wafer background, exposed by scratching the film with a syringe needle, is visible on the right. The thickness of the film was measured by calculating the difference between the average height of the coating and the average height of the background, as shown in Fig. S8(c). In contrast, AFM provided a reliable alternative for thickness measurement, as the line profiles effectively captured the film's surface characteristics and thickness, overcoming the challenges posed by the film's roughness.

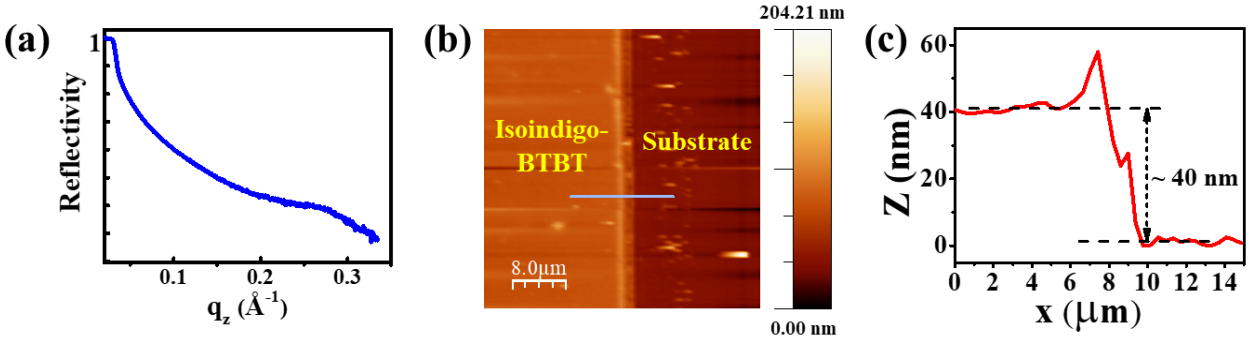

FIG. S9: (a) XRR curve of the Isoindigo-BTBT film at 5 mg/ml concentration, (b) The film thickness measurement by scratching off a portion of the film and scanning using AFM to determine the step height. (c) The line profile drawn at the edge of the film to measure the film thickness.

Thickness measurement of the source and drain electrode of the OFET:

To determine the thickness of the source and drain electrodes XRR measurements were conducted on the thermally evaporated gold film deposited separately on a silicon wafer. The XRR curve of the gold film is presented in FIG. S9. The thickness of the gold film was calculated using the formula $t_{Gold} = \frac{2\pi}{\Delta q_z}$, where $^{\Delta}q_z$ represents the spacing between two successive minima of the Kiessig fringes.

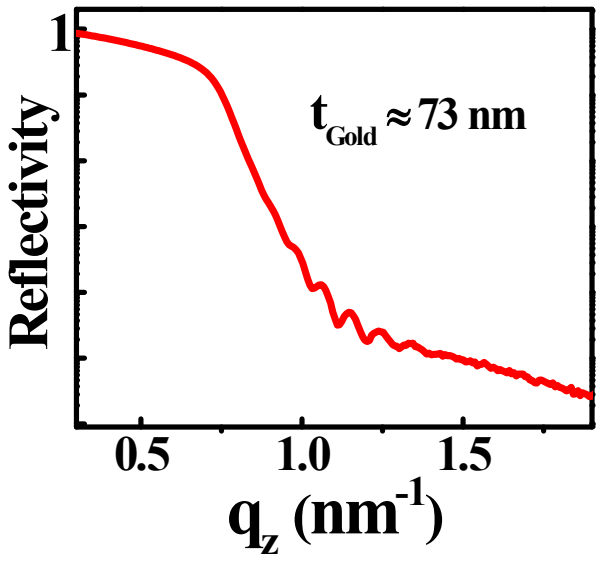

FIG. S10: XRR measurement curve of thermally evaporated 73 nm thick gold film deposited on silicon substrate.

Comparison of Electrical Characteristics of OFETs

We have calculated all key device parameters, including carrier mobility, threshold voltage, and on/off current ratio, which are essential for evaluating the performance of an OFET. A comparison table summarizing these parameters is provided below for reference.

Table: S1

Sl No.	Name	Mobility ($cm^2V^{-1}s^{-1}$)	Threshold Voltage (V)	I_{on}/I_{off}	Ref.
1	P3HT	0.00056	− 30	10^2	(1)
2	E-2Th-BTBT	0.019	− 21	-	(2)
3	2Th-BTBT	0.09	− 15	-	(2)
4	O-2Th-BTBT	0.14	− 28	-	(2)
5	PDBTz1	0.203	− 37	-	(3)
6	PDBTz2	0.198	− 24	-	(3)
7	NDI-BTBT	0.05	10	-	(4)
8	PDI-BTBT	0.11	20	-	(4)

9	Poly (isoindigo-co-bithiophene)	0.0004	− 9.2	10^2	(5)
10	PIBDF-BTO	0.18 ± 0.09	− 44.05	10^2	(6)
11	PI-BTO	0.003 ± 0.0006	− 24.24	10	(6)
12	Thieno [3,2-b] thiophene isoindigo	0.4	-	-	(7)
13	**Isoindigo-BTBT**	**0.001**	**− 32**	**10^2**	**This work**

From the comparison table, it is evident that most conjugated polymer materials exhibit relatively modest charge carrier mobility, similar to our Isoindigo BTBT polymer. However, the underlying reasons for this limitation in mobility have remained largely unexplored in prior research. Our work addresses this critical gap by providing new insights into the structural and molecular factors influencing charge transport, thereby contributing to a deeper understanding of mobility limitations in conjugated polymers.

References:

(1) C.X. Jiang, X.M. Cheng, X.M. Wu, X.Y. Yang, B. Yin, Y.L. Hua, J. Wei, and S.G. Yin, *Optoelectronics Letters* 2011, ***7***, 30—32.

(2) W. Park, C. Yun, S. Yun, J.J. Lee, S. Bae, D. Ho, T. Earmme, C. Kim, and S. Seo, *Journal of Industrial and Engineering Chemistry* 2022, ***114***, 161—170.

(3) S. Doi, T. Mikie, K. Yamanaka, Y. Sato, H. Ohkita, M. Saito, and I. Osaka, . *Polymer Journal* 2024, ***56***, 1051—1059.

(4) S.K. Samanta, I. Song, J.H. Yoo, and J.H. Oh, *ACS Applied Materials & Interfaces* 2018, ***10***, 32444—32453.

(5) A. Hu, A. Nyayachavadi, M. Weires, , G. Garg, S. Wang, and S. Rondeau-Gagné, *RSC Applied Polymers* 2023, ***1***, 292—303.

(6) T. Takaya, M.D. Mamo, M. Karakawa, and Y.Y. Noh, *Journal of Materials Chemistry C* 2018, ***6***, 7822—7829.

(7) T. Lei, J.Y. Wang, and J. Pei, Design, synthesis, and structure–property relationships of isoindigo-based conjugated polymers. *Accounts of chemical research* 2014, ***47***, 1117—1126.